Leggett–Garg inequalities with deformed Pegg–Barnett phase observables

Hiroo Azuma[1],* William J. Munro[1,2], and Kae Nemoto[1,3]
[1] *Global Research Center for Quantum Information Science, National Institute of Informatics, 2-1-2 Hitotsubashi, Chiyoda-ku, Tokyo 101-8430, Japan*
[2] *NTT Basic Research Laboratories and Research Center for Theoretical Quantum Physics, 3-1 Morinosato-Wakamiya, Atsugi, Kanagawa 243-0198, Japan and*
[3] *Okinawa Institute of Science and Technology Graduate University, Onna-son, Okinawa 904-0495, Japan*
(Dated: February 6, 2023)

We investigate the Leggett–Garg inequalities (LGIs) for a boson system whose observables are given by deforming the Pegg–Barnett phase operators. We consider two observables and show that the quantum Fourier transform is useful in the realization of the required measurements. Deriving explicit forms for the LGIs using the coherent state $|\alpha\rangle$ as the initial state, we explore the regimes where they are violated when the time difference between observations of the phase operators is varied. We show that the system remains nonclassical in the large amplitude limit without dissipation, however with dissipation, our violation diminishes rapidly.

arXiv:2207.10900v2 [quant-ph] 3 Feb 2023

I. INTRODUCTION

The Leggett–Garg inequality (LGI) is the temporal analog of Bell's inequality that shows the differences between quantum mechanics and macroscopic local realism [1, 2]. The LGI was proposed to determine how well the following two assumptions work: (1) macroscopic realism and (2) noninvasive measurability. Here macroscopic realism refers to the results of observation that are determined by hidden variables that are qualities of the observed system. The hidden variables are introduced for describing outcomes of any measurement for the system by a deterministic theory instead of quantum mechanics that is nondeterministic [3]. Next noninvasive measurability implies that the result of a measurement at a time t_2 is independent of the result of a previous measurement at time $t_1 (< t_2)$. This means we should be able to perform measurements without disturbing the system. By contrast, quantum mechanics requires an interaction between the system and the observer meaning the system cannot avoid suffering from effects caused by that observer. This means we can regard the noninvasive measurability as a characteristic of classical mechanics. These two assumptions (macroscopic realism and noninvasive measurability) must hold for measurements of classical systems at the macroscopic level.

The above two assumptions for the LGI evoked the following controversies. Maroney and Timpson [4] considered the conflict between quantum theory and macroscopic realism and pointed out that violation of the LGI might not imply the falsity of macroscopic realism at all. To test macroscopic realism, a rigorous experiment of an improved LGI was demonstrated using a superconducting flux qubit [5]. Next [6] insisted that macroscopic realism was a model-dependent notion and constructed a model where invasiveness was controlled by a specific parameter. Then [7] indicated that Fine's proof that Bell's inequalities were necessary and sufficient for the existence of a local realistic model did not hold if we required macroscopic realism [8]. Later [9] demonstrated an experiment that detected the violation of the LGI and excluded macroscopic realism where all superpositions were statistical mixtures in an appropriate basis.

Despite these controversies, considerations about the two assumptions mean that we can expect that a violation of the LGI reveals information about quantum temporal correlations. Further because the LGI is obtained from correlations of the system observed at different times, collapses of the wave function of the system are essential. In other words, the collapse of the wave packet contradicts the noninvasive measurability, so that the LGI must be performed using quantum nondemolition (QND) measurements. In general, QND measurements collapse the wave function unless it is an eigenstate of the observables. In our situation, the system's state is not a state meaning our LGI differs from Bell's inequality in terms of this crucial point [1, 2].

We know that in order to determine an explicit form for our LGI, we need to choose our observable. Which observable we choose is a very difficult problem from a practical point of view. Because the LGI requires QND measurements, a simple quantum circuit for measuring the observable is preferable. So far, the Pauli operators for a qubit system and the displaced parity operators for a boson system have been used as the observables [10, 11]. The LGI for a damped qubit system with Pauli operators as the observables was also explored [10]. Further, the LGI of a

* hiroo.azuma@m3.dion.ne.jp, zuma@nii.ac.jp

boson system weakly coupled to a zero-temperature environment with displacement parity operator observables was shown for a coherent initial state to produce a larger violation than the cat state [11].

Next there have been several experimental demonstrations showing an LGI violation [12–14]. In particular [14], the violation of the LGI for a single photon was detected using linear optical QND measurements [15]. QND measurements are however difficult to efficiently implement. Goggin *et al.* experimentally demonstrated the viiolation of a LGI using the weak measurement of photons as a noninvasive measurement instead of the QND measurement [16]. A relationship between the weak values and the LGI was explored [17]. Finally LGI experiments were undertaken via the modified ideal negative result measurement scheme on a three-level system in liquid-state nuclear magnetic resonance [18].

The systems mentioned above have focused on discrete variable encodings as it had been difficult to find an appropriate Hermitian phase operator for the infinite-dimensional number state Hilbert space [19, 20]. That difficulty arises from the fact that eigenvalues of the number operator are positive or equal to zero and the existence of the vacuum state is significant. Pegg and Barnett steered clear of this trouble by considering the ring-shaped finite-dimensional Hilbert space and set an upper bound of the energy [21–23]. Experimental exploration of the Pegg–Barnett phase operator has been investigated [24–28] with it being measured using photon counting in [24–26]. The uncertainty relation for the phase and photon number of the electromagnetic field in a coherent state of a small average photon number was experimentally estimated with optical homodyne tomography [27, 28]. However, we cannot apply these methods to QND measurements.

In this work, we explore the LGIs for a boson system weakly coupled to a zero-temperature environment. In this scenario, we can exactly solve the master equation of the boson system with a closed-form expression [11, 29, 30]. We consider two deformed Pegg–Barnett operators as observables of the LGI. We show that the quantum Fourier transform (QFT) simplifies the implementation of QND measurements considerably. Further we examine fluctuations of observation of the deformed Pegg–Barnett operator caused by imperfect gates in a quantum circuit of the QFT.

Let us begin by explaining these observables and the time evolution of the LGI in more detail. To define the Pegg–Barnett phase operator in a finite-dimensional Hilbert space, an orthonormal basis is prepared. We construct two pairs of projectors from this orthonormal basis. We build two observables from these projectors (labeled $\hat{O}_s^{(\mathrm{parity})}$ and $\hat{O}_s^{(+,-)}$). Assuming we begin with an initial coherent state and that the boson system evolves under weak interaction with a zero-temperature environment, we can derive explicit forms of the LGIs of these two observables. To estimate the violation of the LGI, we need to measure the observable at different times. We regard the violation of the LGI as a function of the time between the two measurements in the LGI protocol. If we assume that there is no dissipation in the system, the function is periodic. Now to evaluate the quantumness of the system, we compute a dimensionless quantity which is the proportion of the LGI violation in the total period. Next it is important to mention that when dissipation is introduced, the function is not periodic. However, even in this case, we can still compute this quantity. We show that without dissipation, this quantity remains at a nonzero value and the violation of the LGI does not vanish in a specific limit. By contrast, if the system has dissipation, the violation of the LGI disappears and the dimensionless quantity converges to zero as the degree of the dissipation becomes larger. This is one of the major results of our work.

Now to the structure of this paper. It is organized as follows. In Sec. II, we provide the theoretical backgrounds for our model, the LGI, and the Pegg–Barnett phase operator. Next in Sec. III, we define the observables for the LGIs by deforming the Pegg–Barnett phase operator while in Sec. IV, we discuss the implementation of measurements of the deformed Pegg–Barnett operators using the QFT. In Sec. V, we evaluate dissipation of measurements of an imperfect quantum circuit of the QFT while in Sec. VI, we derive an explicit form of the LGI with $\hat{O}_s^{(\mathrm{parity})}$ and provide its numerical evidence. In Sec. VII, we derive an explicit form of the LGI with $\hat{O}_s^{(+,-)}$ and provide its numerical evidence. Finally in Sec. VIII, we provide a concluding discussion and summary of our results.

II. THEORETICAL BACKGROUND

Before we proceed to our main results let us provide some preliminary materials beginning with our model. Consider the following master equation of a boson system coupled weakly to a zero-temperature environment:

$$\dot{\rho}(t) = -i\omega[a^\dagger a, \rho(t)] + \Gamma\Big(2a\rho(t)a^\dagger - a^\dagger a\rho(t) - \rho(t)a^\dagger a\Big), \tag{1}$$

where a and $a^\dagger$ are the annihilation and creation operators of the boson system, Γ is the decay rate, and ω is the angular frequency of the boson system. Here, we draw attention to the fact that we do not work in the interaction picture where we could eliminate the Hamiltonian term. Instead we will work in the Schrödinger picture. The decay rate Γ and the angular frequency of the boson system ω have the dimension of reciprocal time. In Appendix A, we explicitly show the solution of such a master equation.

Next, the LGI is defined as follows. First, we consider an operator $\hat{O}$ whose eigenvalues are given by ± 1. Second, we introduce three equally spaced measurement times, $t_1 = 0$, $t_2 = \tau$, and $t_3 = 2\tau$ with $\tau > 0$. Third, we describe an observed value of $\hat{O}$ at t_i as O_i. Fourth, we write the probability that we obtain observed values O_i and O_j at times t_i and $t_j (> t_i)$ respectively as $P_{ij}(O_i, O_j)$. Fifth, we define the correlation function C_{ij} as

$$C_{ij} = \sum_{O_i, O_j \in \{-1, +1\}} O_i O_j P_{ij}(O_i, O_j). \tag{2}$$

Finally, we can write the LGI as follows:

$$-3 \leq K_3 = C_{12} + C_{23} - C_{13} \leq 1. \tag{3}$$

Now to define the Pegg–Barnett phase operator [21–23], we consider the following state vectors:

$$|\phi_m\rangle_s = (s+1)^{-1/2} \sum_{n=0}^{s} \exp[in\phi_m]|n\rangle, \tag{4}$$

where

$$\phi_m = \phi_0 + \frac{2\pi}{s+1} m \quad \text{for } m = 0, 1, 2, ..., s, \tag{5}$$

and $\{|n\rangle : n = 0, ..., s\}$ are Fock number states. The vectors $\{|\phi_m\rangle_s : m = 0, 1, 2, ..., s\}$ form a complete orthonormal system in the $(s+1)$-dimensional Hilbert space. Then, the Pegg–Barnett phase operator can be defined as [21–23]:

$$\hat{\phi} = \sum_{m=0}^{s} \phi_m |\phi_m\rangle_{ss}\langle\phi_m|. \tag{6}$$

III. OBSERVABLES FROM THE DEFORMED PEGG–BARNETT PHASE OPERATOR

We can use the basis $\{|\phi_m\rangle_s\}$ to define two observables, $\hat{O}_s^{(\text{parity})}$ and $\hat{O}_s^{(+,-)}$ which are given by

$$\hat{O}_s^{(\text{parity})} = \Pi_s^{(\text{even})} - \Pi_s^{(\text{odd})}, \tag{7}$$

$$\hat{O}_s^{(+,-)} = \Pi_s^{(+)} - \Pi_s^{(-)}, \tag{8}$$

with

$$\Pi_s^{(\text{even})} = \sum_{m=0}^{N} |\phi_{2m}\rangle_{ss}\langle\phi_{2m}|, \quad \Pi_s^{(\text{odd})} = \sum_{m=0}^{N} |\phi_{2m+1}\rangle_{ss}\langle\phi_{2m+1}|, \tag{9}$$

$$\Pi_s^{(+)} = \sum_{m=0}^{N} |\phi_m\rangle_{ss}\langle\phi_m|, \quad \Pi_s^{(-)} = \sum_{m=N+1}^{2N+1} |\phi_m\rangle_{ss}\langle\phi_m|. \tag{10}$$

Here $s = 2N + 1$ with $N = 0, 1, 2, ...$ Remembering that $\{|\phi_m\rangle_s\}$ form a complete orthonormal basis, the eigenvalues of $\hat{O}_s^{(\text{parity})}$ and $\hat{O}_s^{(+,-)}$ must be either ± 1. Now in our work here we will let s be large but not infinite. Because the right-hand side of Eq. (4) is divided by $\sqrt{s+1}$, some might worry whether taking the large s limit is allowed. However, a relationship $\text{Tr}[\Pi_s^{(\text{even})}] = \text{Tr}[\Pi_s^{(\text{odd})}] = \text{Tr}[\Pi_s^{(+)}] = \text{Tr}[\Pi_s^{(-)}] = 1/2$ holds rigorously, so that the factor $(s+1)^{-1/2}$ does not cause issues.

IV. MEASUREMENTS WITH THE OBSERVABLES $\hat{O}_s^{(\text{parity})}$ AND $\hat{O}_s^{(+,-)}$

If we carry out measurements with the projection operators constructed from $\{|\phi_m\rangle_s\}$, we can perform measurements with $\hat{O}_s^{(\text{parity})}$ and $\hat{O}_s^{(+,-)}$. Although this method is not always optimal for determining $\hat{O}_s^{(\text{parity})}$ and $\hat{O}_s^{(+,-)}$, we will

proceed in that direction as it gives us a clear perspective. From Eq. (4), we can regard the vector $|\phi_m\rangle_s$ as a superposition of the boson system's number states $\{|n\rangle : n = 0, 1, ..., s\}$. Here, we set $s = d - 1$ with $d = 2^L$. Remembering that $s = 2N + 1$, we have $N = (d/2) - 1$. If we put $L = 1, 2, 3, 4, ...$, we need to set $s = 1, 3, 7, 15, ...$ This in turn obviously means the dimension of the Hilbert space on which $\hat{O}_s^{(\mathrm{parity})}$ and $\hat{O}_s^{(+,-)}$ are defined is restricted by the number of qubits for the QFT.

We can now consider the following unitary transformation that maps a number state of the boson system to a state of L qubits:

$$U : |x\rangle \to |x_1\rangle|x_2\rangle...|x_L\rangle \quad \text{for } x = 0, 1, ..., d - 1, \tag{11}$$

with $x_i \in \{0, 1\}$ for $i = 1, 2, ..., L$ and $x = \sum_{i=1}^{L} x_i 2^{L-i}$.

Realization of this transformation U is challenging and beyond the scope of the article. By postulating the existence of U, we can realize measurements of $\hat{O}_s^{(\mathrm{parity})}$ and $\hat{O}_s^{(+,-)}$ however as follows. First, we consider the QFT of L qubits [31, 32],

$$\mathrm{QFT} : |x\rangle \to \frac{1}{\sqrt{d}} \sum_{y=0}^{d-1} \exp[i(2\pi/d)xy]|y\rangle, \tag{12}$$

for $x = 0, 1, ..., d - 1$. Second, we apply the QFT to $|\phi_m\rangle_s$ as follows:

$$\mathrm{QFT} : |\phi_m\rangle_s \to \frac{1}{d} \sum_{y=0}^{d-1} \frac{1 - \exp(izd)}{1 - \exp(iz)}|y\rangle, \tag{13}$$

$$z = \phi_0 + \frac{2\pi}{d}(y + m). \tag{14}$$

We draw attention to the fact that the $\sqrt{s+1}$ part in Eq. (4) has been integrated into a factor $1/d$ in the right-hand side of Eq. (13) because $s+1 = d$. The right-hand side of Eq. (13) has sharp peaks around $z = 0$. Thus, if we observe the right-hand side of Eq. (13), we obtain $|y\rangle$ with a probability of almost unity where y is the nearest integer of $\{-m - [d/(2\pi)]\phi_0\}$. Hence, if we put $\phi_0 = 0$, $y = m$ holds. Therefore, the QFT maps each $|\phi_m\rangle_s$ into a computational basis vector $|m\rangle$ for $m = 0, 1, ..., d - 1$. This implies that we can identify $|\phi_m\rangle_s$ with ease.

Now to observe the observable $\hat{O}_s^{(\mathrm{parity})}$, we need to measure only one qubit $|y_1\rangle$ among the L qubits. This is because we must only distinguish whether $y = \sum_{i=1}^{L} y_i 2^{L-i}$ is odd or even. In contrast, to observe the observable $\hat{O}_s^{(+,-)}$, we have to measure only one qubit $|y_L\rangle$ among the L qubits. This is because we must only distinguish whether or not y is smaller than $N + 1 = d/2$. The fact that we can observe $\hat{O}_s^{(\mathrm{parity})}$ and $\hat{O}_s^{(+,-)}$ by detecting only the one qubit gives us a great advantage in carrying out the QND measurements. Next Fig. 1 (a) shows how to perform the QND measurement of $\hat{O}_s^{(\mathrm{parity})}$. First, we apply the QFT to a state $|\psi\rangle = \sum_m c_m|\phi_m\rangle_s$ followed by measuring $|y_1\rangle$ in the basis $\{|0\rangle, |1\rangle\}$. Then we insert $|0\rangle$ or $|1\rangle$ into the first qubit according to the result of the measurement leaving $(L - 1)$ qubits untouched, and feed all of the qubits into the inverse QFT. Finally, we obtain a wave packet that is generated by a collapse, $\Pi_s^{(\chi)}|\psi\rangle/\sqrt{\langle\psi|\Pi_s^{(\chi)}|\psi\rangle}$ for $\chi \in \{\mathrm{even}, \mathrm{odd}\}$. We can perform the QND measurement with $\hat{O}_s^{(+,-)}$ similarly.

As mentioned before, one of the research tasks from now on is finding out how to implement the unitary transformation U given by Eq. (11). We cannot omit it before performing the QFT. We do not examine a method for the realization of this boson–qubit transformation U in detail because it is very difficult and lies outside the scope of our study.

V. ERRORS AND IMPERFECTIONS IN THE MEASUREMENT OF $\hat{O}_s^{(+,-)}$

The quantum circuit that carries out the QFT is composed of the Hadamard gates and controlled phase shift gates and so in Fig. 1 (b) we show an illustrative three-qubit QFT. In general, for most of the suggested realizations, for example, trapped ion quantum computers, the single-qubit operations are faster than the conditional gates for two-qubit operations which has implications in terms of errors and imperfections. We can assume that the conditional phase shift gates are more vulnerable to decoherence than the Hadamard gates [33] and so it is convenient for illustrative purposes to introduce random noise only to the conditional phase shift gates. For example, letting $|x\rangle_1$

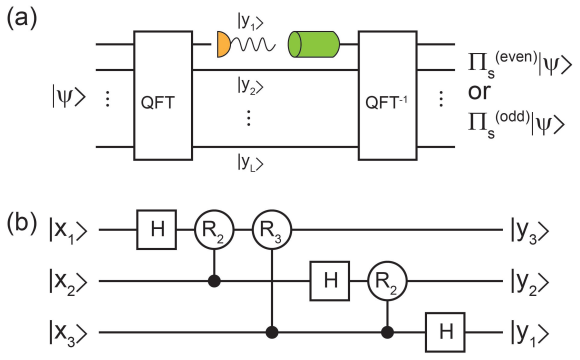


FIG. 1. (a) Schematic of the QND measurement with $\hat{O}_s^{(\mathrm{parity})}$. (b) Quantum circuit of three-qubit QFT. The Hadamard gate and the controlled phase shift gate are represented by H and R_k, respectively. Here, R_k rotates the phase by $2\pi/2^k$.

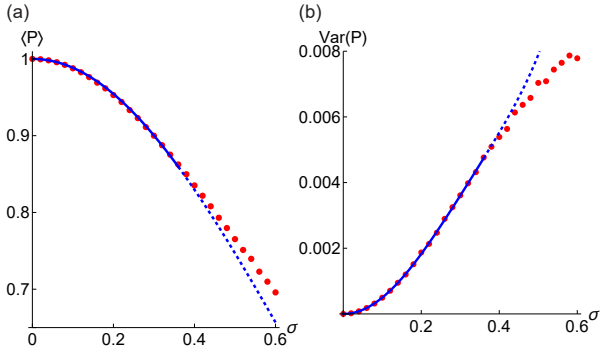


FIG. 2. Monte Carlo simulations of $\langle P\rangle$ and $\mathrm{Var}(P)$. In (a) we plot $\langle P\rangle$ as a function of σ where the red points represent simulation results. Because an error of each result is within $\pm 2.6\times 10^{-3}$, we do not put error bars onto our simulation points. Our approximate solution given by Eq. (24) is shown with the solid blue curve for $0\le\sigma\le 0.36$ and the dashed blue curve for $0.36\le\sigma\le 0.6$. (b) Plot of the $\mathrm{Var}(P)$ as a function of σ. Because an error of each result is within $\pm 2.5\times 10^{-4}$, we do not put error bars onto our simulation points. Our approximate solution from Eq. (25) is depicted with the solid blue curve for $0\le\sigma\le 0.36$ and the dashed blue curve for $0.36\le\sigma\le 0.6$. For both the plots shown in (a) and (b), the fitted curves of Eqs. (24) and (25) are effective for small σ, that is, $0\le\sigma\le 0.36$. This is because these approximate curves are reliable under perturbation theory. As explained before the noisy C-R_k is useful for $\Delta_{pq}<2\pi/d=2\pi/2^L$. Because we put $L=5$, the fitting parameters c_0, c_1, c_2, and c_3 are trustworthy for $\sigma<2\pi/d=0.196$.

and $|y\rangle_2$ represent the first and second qubits and regarding them as the control and target qubits respectively, we can describe an imperfect conditional phase shift gate as

$$\text{noisy C-}R_k:|x\rangle_1|y\rangle_2\to\begin{cases}|x\rangle_1|y\rangle_2 & \text{for } (x,y)\neq(1,1)\\ \exp[(i2\pi/2^k)+i\Delta_{12}]|x\rangle_1|y\rangle_2 & \text{for } (x,y)=(1,1)\end{cases}, \tag{15}$$

where Δ_{12} is a Gaussian random variable with mean zero and variance σ^2 whose probability is given by

$$P(\Delta_{12})=\frac{1}{\sqrt{2\pi}\sigma}\exp\Big[-\frac{\Delta_{12}^2}{2\sigma^2}\Big]. \tag{16}$$

It is then straightforward to obtain the noisy QFT for L qubits as

$$\text{noisy QFT}:|x\rangle\to\frac{1}{\sqrt{d}}\sum_{y=0}^{d-1}\exp\left[i(2\pi/d)xy+i\sum_{\substack{p\in\{2,\ldots,L\},\\ q\in\{1,\ldots L-1\},\\ p>q}}\Delta_{pq}x_p y_{L-q+1}\right]|y\rangle. \tag{17}$$

To estimate the variance of the probability of the wave packets obtained by measurements of $\hat{O}_s^{(+,-)}$ with the imperfect QFT, we need to define our initial state. We use the following L-qubit state that is similar to the coherent state:

$$|\alpha\rangle_s=C_s(\alpha)\sum_{x=0}^{d-1}\frac{\alpha^x}{\sqrt{x!}}|x\rangle, \tag{18}$$

$$C_s(\alpha)=\left(\sum_{x=0}^{d-1}\frac{|\alpha|^{2x}}{x!}\right)^{-1/2}. \tag{19}$$

We draw attention to the fact that the normalization factor $C_s(\alpha)$ depends on $s = d - 1$ because $|\alpha\rangle_s$ lies on $(s+1)$-dimensional Hilbert space.

Now let us consider the time evolution of $|\alpha\rangle_s$ as follows. First, the noisy QFT transforms $|\alpha\rangle_s$ as

$$|\psi\rangle_s = (\text{noisy QFT})|\alpha\rangle_s. \tag{20}$$

Noting that we want to observe $\hat{O}_s^{(+,-)}$, we should therefore measure $|y_L\rangle$. If we detect $y_L = 0$ corresponding to $O_s^{(+,-)} = 1$, the wave function collapses from $|\psi\rangle_s$ to the non-normalized state

$$|\psi_+\rangle_s = |y_L = 0\rangle\langle y_L = 0|\psi\rangle_s, \tag{21}$$

where $|y_L = 0\rangle\langle y_L = 0|$ is a one-qubit projector. In contrast, if we detect $y_L = 1$ corresponding to $O_s^{(+,-)} = -1$, the wave function collapses from $|\psi\rangle_s$ to the non-normalized state

$$|\psi_-\rangle_s = |y_L = 1\rangle\langle y_L = 1|\psi\rangle_s. \tag{22}$$

Explicit forms of $|\psi\rangle_s$ and $|\psi_\pm\rangle_s$ are given in Appendix B.

Although we are examining decoherence, we describe states that suffer from noises of imperfect gates as pure states, $|\psi_+\rangle_s$ and $|\psi_-\rangle_s$. This is because the error of the noisy conditional phase shift gate is introduced by the unitary operation. However, it is all right because the states will become mixed by carrying out many runs for the Monte Carlo simulations. To accomplish the QND measurements, we need to apply $(\text{noisy QFT})^{-1}$ to $|\psi_\pm\rangle_s$ as

$$|\psi'_\pm\rangle_s = (\text{noisy QFT})^{-1}|\psi_\pm\rangle_s. \tag{23}$$

Explicit forms of $|\psi'_\pm\rangle_s$ are given in Appendix B.

Now to evaluate the noisy operation on our measurement of $\hat{O}_s^{(+,-)}$, we consider the following probability:

$$P(\sigma) = |{}_s\langle\psi'_+(\Delta_{pq} = \tilde{\Delta}_{pq} = 0)|\psi'_+(\Delta_{pq}, \tilde{\Delta}_{pq})\rangle_s + {}_s\langle\psi'_-(\Delta_{pq} = \tilde{\Delta}_{pq} = 0)|\psi'_-(\Delta_{pq}, \tilde{\Delta}_{pq})\rangle_s|^2,$$

where $\{\Delta_{pq}\}$ and $\{\tilde{\Delta}_{pq}\}$ are Gaussian variables generated by the noisy QFT and $(\text{noisy QFT})^{-1}$ respectively, and the relationships between σ and $\{\Delta_{pq}, \tilde{\Delta}_{pq}\}$ are given by Eq. (16). Obviously, $P(\sigma = 0) = 1$ holds. We can now define the average and variance of $P(\sigma)$ as $\langle P\rangle$ and $\text{Var}(P) = \langle(P - \langle P\rangle)^2\rangle$, respectively. We obtain $\langle P\rangle$ and $\text{Var}(P)$ using Monte Carlo simulations with 2×10^4 samples for the $L = 5$ qubit case with $\alpha = 1/2$. In Figs. 2 (a) and (b), we plot the average and the variance as functions of σ, respectively. Fitting the function $\langle P\rangle = \exp(-c_0\sigma^2)$ chosen due to the rotational error's nature to the red data points shown in Fig. 2 (a) for $0 \le \sigma \le 0.36$, we obtain

$$c_0 = -1.168 \pm 0.0023, \tag{24}$$

as an approximation. This approximation holds for small σ. Looking at Eq. (15), we notice that the error of the conditional phase shift gate is crucial when $\Delta_{pq} \sim 2\pi/d$. Because of $L = 5$ and Eq. (16), we estimate the typical σ at $2\pi/2^5 = 0.196$.

In Fig. 2 (b), we show our numerical results for $\text{Var}(P)$ by the red dots. Fitting a polynomial function $\text{Var}(P) = c_1\sigma^2 + c_2\sigma^4 + c_3\sigma^6$ to the data points for $0 \le \sigma \le 0.36$, we obtain

$$\begin{aligned} c_1 &= 0.051\,22 \pm 0.001\,127, \\ c_2 &= -0.1499 \pm 0.034\,59, \\ c_3 &= 0.2850 \pm 0.2514. \end{aligned} \tag{25}$$

We can witness similar effects for the measurements of the operator $\hat{O}_s^{(\text{parity})}$.

VI. DERIVATION OF THE LGI OF THE OBSERVABLE $\hat{O}_s^{(\text{parity})}$

Let us now turn our attention to the LGIs and their potential violation. We start by preparing the coherent state $|\alpha\rangle$ as our initial state of the system at $t_1 = 0$. Choosing $\hat{O}_s^{(\text{parity})}$ as our observable and based on the details presented in Appendix C we can obtain the correlation function C_{12} as

$$C_{12} = \exp[-|\alpha|^2]\text{Re}\Big[\text{Tr}[\Pi_s^{(\text{even})}(L_1(\tau) + L_2(\tau))] - \text{Tr}[\Pi_s^{(\text{odd})}(L_1(\tau) + L_2(\tau))]\Big], \tag{26}$$

where

$$\begin{aligned}
&\mathrm{Tr}[\Pi_s^{(\mathrm{even})}(L_1(\tau)+L_2(\tau))]-\mathrm{Tr}[\Pi_s^{(\mathrm{odd})}(L_1(\tau)+L_2(\tau))]\\
&=\sum_{n=0}^{N}\{\frac{|\alpha|^{2n}}{n!}\exp[i\omega(N+1)\tau]+\frac{|\alpha|^{2(n+N+1)}}{(n+N+1)!}\exp[-i\omega(N+1)\tau]\}\\
&\times\exp[-\Gamma\tau(2n+N+1)]\sum_{l=0}^{n}\Big[\exp[2\Gamma t]-1\Big]^{l}\sqrt{\begin{pmatrix}n+N+1\\ l\end{pmatrix}\begin{pmatrix}n\\ l\end{pmatrix}},
\end{aligned}\tag{27}$$

and $L_1(\tau)$ and $L_2(\tau)$ are given by Eqs. (C15) and (C16), respectively. In Eq. (26), the real part of Eq. (27) remains with the reason given in Appendix C. From Eqs. (26) and (27), we can compute C_{12}. We draw attention to the fact that C_{12} does not depend on ϕ_0. Instead it is a function of variables N, τ, α, Γ, and ω, that is to say, $C_{12}(N,\tau,\alpha,\Gamma,\omega)$. We can then obtain C_{13} and C_{23} as

$$C_{13}=C_{12}(N,2\tau,\alpha,\Gamma,\omega),\tag{28}$$

$$C_{23}=C_{12}(N,\tau,\alpha\exp(-i\Omega\tau),\Gamma,\omega),\tag{29}$$

where we used Eq. (A1). These correlations functions thus enable us to determine K_3.

It is now useful to numerically explore the behavior of K_3 using $\hat{O}_s^{(\mathrm{parity})}$ as our measurement observable with $|\alpha\rangle$ as our initial state. Figure 3 (a) shows graphs of K_3 without dissipation as a function of τ. The maximum value of K_3 in Fig. 3 (a) is equal to 3/2 with very small numerical errors. In Fig. 3 (b), we plot a graph of K_3 as a function of τ with nonzero Γ. The amplitude of oscillations of the graph decreases gradually as τ becomes larger until we reach a stage when the LGI is not violated.

The plots shown in Fig. 3 are very typical for the LGI. The time evolution of a qubit whose Hamiltonian was proportional to σ_x exhibited the violation of the LGI and its graph as a function of τ was very similar to Fig. 3 (a) [2]. In Ref. [34], the violation of the LGI for an optoelectromechanical system was investigated and its graph as a function of τ showed modulation caused by the non-energy-conserving terms in interaction. In this study, the graph resembled Fig. 3 (b), as well.

Next [35] showed that the LGI was violated for systems with arbitrary spin lengths. References [35] and[36] pointed out that the time evolution with either decoherence or coarse-grained measurements increased classical properties and undermined the violation of the LGI. These considerations were consistent with Fig. 3 (b). Then [37] discussed that the quantum bound of the violation of the LGI depended on the number of levels of the system. In the limit where the number of levels got closer to infinity, the violation of the LGI approached the algebraic maximum. In these references, the LGI for spin systems was investigated. Figure 3 tells us that the violation of the LGI for the boson system reveals similar properties to multilevel systems. However, as mentioned before, the realization of the QND measurements for the boson system is very difficult compared to that of the multilevel systems. This is because we can hardly implement the unitary transformation U defined in Eq. (11). Reference [2] introduced an experiment of the LGI with a superconducting transmon qubit [13]. In summary, the QND measurements of spin systems have already been viable tasks. By contrast, counting the number of photons in a QND manner is a difficult task in the future.

VII. DERIVATION OF THE LGI OF THE OBSERVABLE $\hat{O}_s^{(+,-)}$

Similar to our procedure for the parity observable we can determine what happens for $\hat{O}_s^{(+,-)}$ as well when using the initial coherent state $|\alpha\rangle$. Choosing $\hat{O}_s^{(+,-)}$ as the observable, based on calculations given in Appendix D, we can describe the correlation function C_{12} as

$$C_{12}=4\exp[-|\alpha|^2]\mathrm{Re}\Big[\mathrm{Tr}[\Pi_s^{(+)}L(\tau)]-\mathrm{Tr}[\Pi_s^{(-)}L(\tau)]\Big],\tag{30}$$

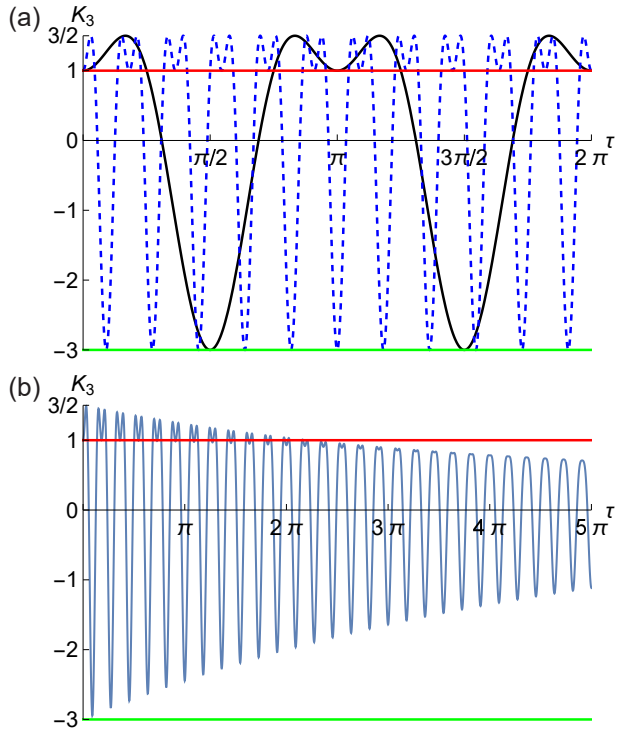


FIG. 3. Plots of K_3 as functions of τ. In (a) we have set $\phi_0 = 0$, $\alpha = 1/2$, $\Gamma = 0$, and $\omega = 1$. The solid black and dashed blue curves represent $N = 1$ and $N = 10$, respectively. A period of the graphs is equal to $2\pi/(N + 1)$. The red and green lines represent $K_3 = 1$ and $K_3 = -3$, respectively. These graphs suggest that the period of the curve of $N = 1$ is $11/2$ times longer than that of the curve of $N = 10$. In (b) we have set $N = 10$, $\phi_0 = 0$, $\alpha = 1/2$, $\Gamma = 0.005$, and $\omega = 1$.

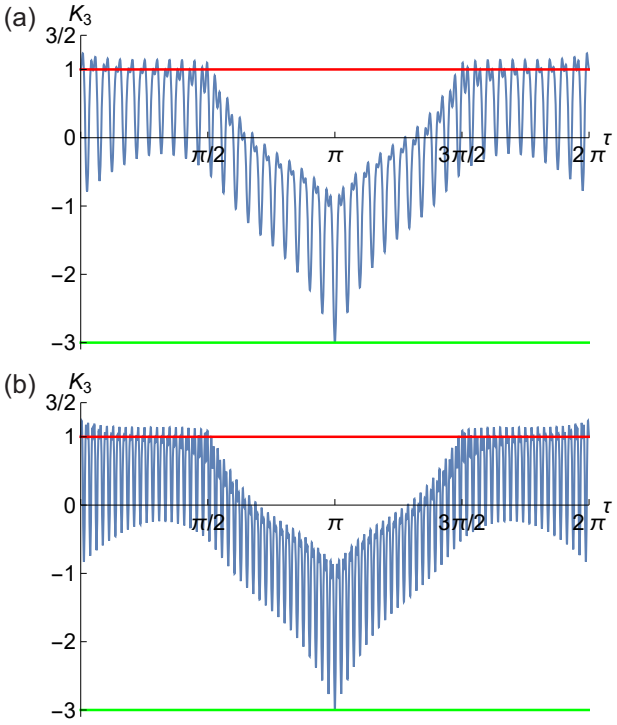


FIG. 4. Plots of K_3 as a function of τ with $\phi_0 = 0$, $\alpha = 1/2$, $\Gamma = 0$ and $\omega = 1$ for (a) $N = 20$, (b) $N = 40$.

where

$$\begin{aligned}
&\mathrm{Tr}[\Pi_s^{(+)} L(\tau)] - \mathrm{Tr}[\Pi_s^{(-)} L(\tau)] \\
&= 4(s+1)^{-2} \sum_{m=0}^{s} \sum_{\substack{m'=0, \\ m-m'=\text{odd}}}^{s} \sum_{\substack{n=0, \\ n-m'=\text{odd}}}^{s} \frac{\exp[-i(n-m)\phi_0]}{\{\exp[-i(n-m')\pi/(N+1)] - 1\}\{\exp[i(m-m')\pi/(N+1)] - 1\}} \\
&\times \frac{\alpha^n \alpha^{*m}}{\sqrt{n!m!}} \exp[-\Gamma\tau(n+m') - i\omega(n-m')\tau] \sum_{l=0}^{\min(n,m')} \Big[\exp[2\Gamma\tau] - 1\Big]^l \sqrt{\binom{n}{l}\binom{m'}{l}},
\end{aligned} \tag{31}$$

and $L(\tau)$ is given by Eq. (D15). Similarly to the previous situation we can obtain C_{13} and C_{23} as

$$C_{13} = C_{12}(N, 2\tau, \phi_0, \alpha, \Gamma, \omega), \tag{32}$$

$$C_{23} = C_{12}(N, \tau, \phi_0, \alpha \exp(-i\Omega\tau), \Gamma, \omega), \tag{33}$$

allowing us to determine K_3.

Figures 4 (a), (b) show plots of K_3 as functions of τ for $N = 20$ and 40, respectively. Looking at these we note that oscillations of the graph increase as N becomes larger. Amplitudes of oscillations of short periods in the graph do not decrease even if N becomes larger. Thus, we can expect that a graph of K_3 as a function of τ contains oscillations of infinitely high frequency as $N \to \infty$. Further Figs. 5 (a), (b) show plots of K_3 as functions of τ for two different dissipation values, namely $\Gamma = 0.005$ and 0.1, respectively. Looking at these plots we note that the amplitude of the oscillations of K_3 decreases as Γ becomes larger. More specifically looking at Fig. 5 (b), we note that K_3 converges to zero as τ increases on condition $\Gamma > 0$.

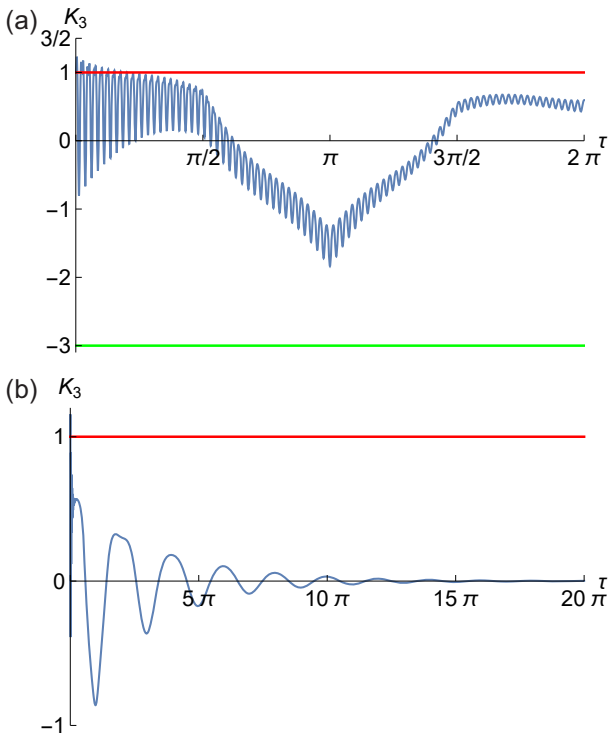


FIG. 5. Plots of K_3 as a function of τ with $N = 40$, $\phi_0 = 0$, $\alpha = 1/2$ and, $\omega = 1$ for (a) $\Gamma = 0.005$, (b) $\Gamma = 0.1$. The value K_3 converges to zero as τ becomes larger in (b).

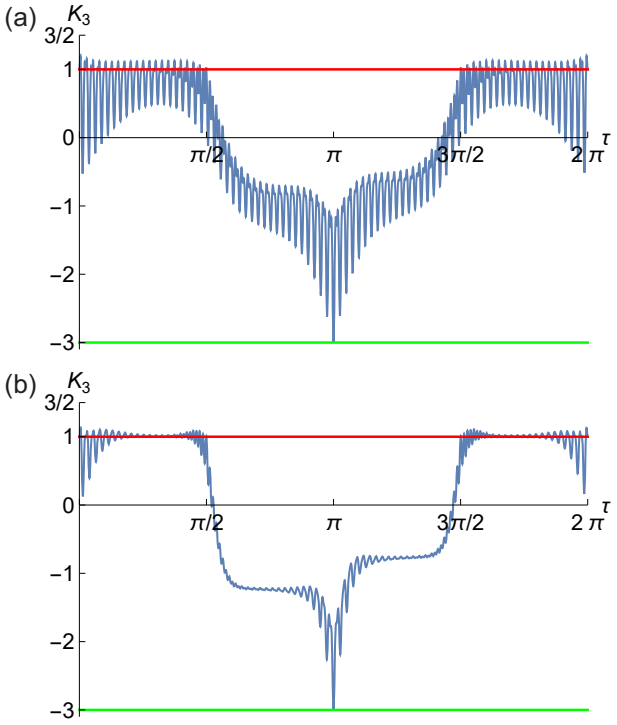


FIG. 6. Plots of K_3 as a function of τ with $N = 40$, $\phi_0 = 0$, $\Gamma = 0$ and, $\omega = 1$ for (a) $\alpha = 1$, (b) $\alpha = 2$.

Next Figs. 6 (a), (b) shows plots of K_3 as functions of τ for $\alpha = 1$ and 2, respectively. Figure 7 shows plots of K_3 as a function of τ for $N = 100$, 200, and 1000. As N becomes larger, the curves approach a step function

$$f(\tau) = \begin{cases} 1 & \text{for } 0 \le \tau < \pi/2 \text{ and } 3\pi/2 \le \tau < 2\pi \\ -1 & \text{for } \pi/2 \le \tau < 3\pi/2 \end{cases} . \tag{34}$$

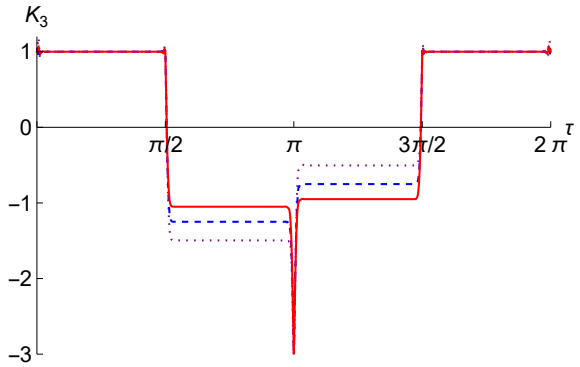


FIG. 7. Plots of K_3 as a function of τ for various N with $\phi_0 = 0$, $\alpha = 10$, $\Gamma = 0$, and $\omega = 1$. The dotted purple, dashed blue, and solid red curves represent $N = 100$, 200, and 1000, respectively.

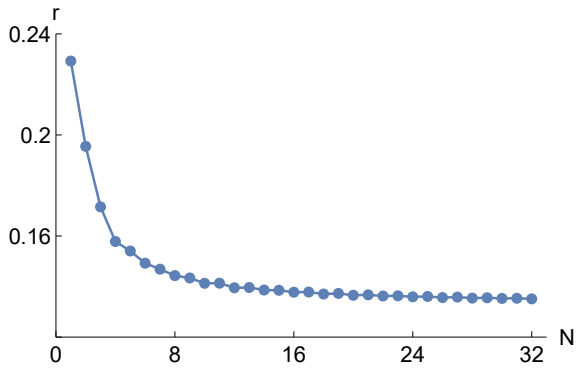


FIG. 8. Plot of the proportion r as a function of N for $\phi_0 = 0$, $\alpha = 1/2$, $\Gamma = 0$, and $\omega = 1$.

We can now compute the proportion of the time cycle where the LGI is violated. This we term the r value and it is calculated as follows. Starting with the dissipationless case, the period of K_3 as a function of τ is equal to $2\pi/\omega$. We can then divide this period into M slices of size $\Delta\tau = 2\pi/(M\omega)$. Within each slice we examine whether or not the

LGI is violated at each $\tau_m = m\Delta\tau$ for $m = 0, 1, 2, ..., M$. We count the number of slices $\tilde{M}$ where the LGI is violated. Strictly speaking $0 \leq \tilde{M} \leq M$. Finally, we define the dimensionless ratio r as

$$r = \tilde{M}/M. \tag{35}$$

This ratio was defined for the dissipationless case but can also be used when dissipation is present. In this case we set $\Delta\tau = 2\pi/(M\omega)$, and can determine r as previously described. We can regard r as the proportion of the LGI violation and explore its behavior.

Figure 8 shows a plot of r as a function of N. The period of K_3 for τ is equal to 2π and we divide the period into $M = 10^6$ slices of size $2\pi/M$. Looking at Fig. 8, we note that r approaches 0.137 as N becomes larger. The graph of Fig. 8 suggests that the violation is preserved as N increases in the dissipationless case. However, if Γ is not equal to zero we observe as seen in Fig. 9, the violation is getting smaller and r approaches zero exponentially.

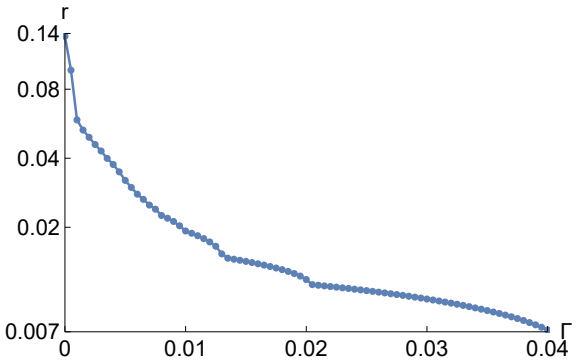


FIG. 9. Plot of the proportion r as a function of Γ for $\phi_0 = 0$, $\alpha = 1/2$, $N = 25$, and $\omega = 1$. The proportion r is displayed on a logarithmic scale.

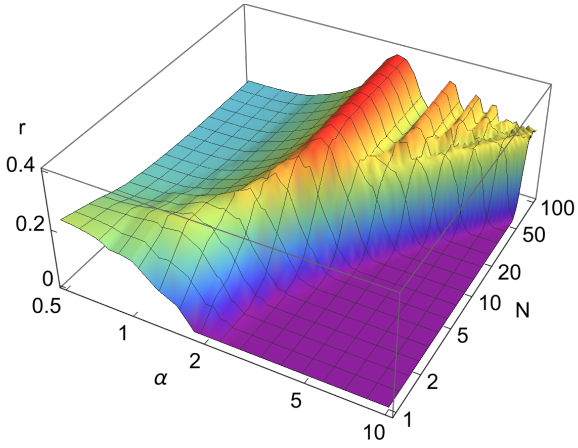


FIG. 10. Plot of the proportion r as a function of real α and N for $\phi_0 = 0$, $\Gamma = 0$, and $\omega = 1$. The axes of α and N are displayed on a logarithmic scale.

Next Fig. 10 shows a three-dimensional plot of r as a function of both α and N. Here we assume α is real. We observe from the plot that r does not approach zero in a large α and N limit. In the dissipationless case the violation of the LGI does not disappear as N increases even if α is large enough. If we let $|\alpha|$ and N become large the graph of K_3 can be approximated by the step function of Eq. (34) implying the violation of the LGI remains.

In Fig. 10, we have shown that the LGI of the coherent state $|\alpha\rangle$ reveals the violation in a large N limit even if we let $|\alpha|$ be large. Because

$$\frac{2\Delta n \Delta\phi}{|\langle\alpha|[\hat{n}, \hat{\phi}]|\alpha\rangle|} \simeq 1 \tag{36}$$

holds for $|\alpha| \gg 1$ where $\hat{n}$ is the number operator of bosons and $\hat{\phi}$ is the Pegg–Barnett phase operator defined in Eq. (6) with $s \to \infty$, the coherent state $|\alpha\rangle$ shows the minimum uncertainty [30, 38]. However, Fig. 10 tells us that large $|\alpha|$ reveals the violation of the LGI. Thus, $|\alpha\rangle$ keeps its nonclassical properties and it cannot be described with classical theory.

Next as shown in Figs. 5 (b) and 9, if we introduce dissipation, K_3 approaches zero as τ becomes larger and r decreases exponentially as Γ becomes larger. It was reported that quantum properties of a damped two-level system decay exponentially in time because of the coupling to the thermal reservoir [10]. In the current paper, we assume that there is no thermal fluctuation of the external reservoir but the boson system suffers from dissipation due to the interaction with the zero-temperature environment. In this scenario, we show the exponential decay of the LGI. Thus, we can conclude that the interaction with the external system causes the reduction of quantumness, for example, the violation of the LGI, for the system.

The shape of the graph in Fig. 4 (a) is very different from that in Fig. 3 (a). We can recognize the plot of Fig. 4 (a) as an isolated one because Fig. 3 (a) is common for the graphs of the LGI, for example, as shown in Ref. [2]. It surprises us that difference of observables $\hat{O}_s^{(\mathrm{parity})}$ and $\hat{O}_s^{(+,-)}$ generates the difference between Figs. 3 (a) and 4 (a). Moreover, the graph of Fig. 4 (a) changes into the step function shown in Figs. 6 and 7 under the large $|\alpha|$ and N limit. Thus, the choice of $\hat{O}_s^{(+,-)}$ for the LGI provides us with plenty of physical meanings.

In Fig. 10 we evaluated the proportion r in the range $0.5 \leq \alpha \leq 10$ with $1 \leq N \leq 100$. By letting α and N become larger, we witness an oscillation of r. This phenomenon remains to be investigated more precisely in the future.

VIII. CONCLUSIONS AND DISCUSSIONS

As mentioned in our introduction, a violation of the LGI shows that there is a difference between quantum mechanics and macroscopic local realism. Microscopic systems obviously tend to have a quantum nature and as such it is thus important to explore systems involving large particle/photon numbers. Boson systems are interesting in that respect as one can easily create quantum states of light with varying mean photon number. The simplest of course is the coherent state $|\alpha\rangle$ which is often considered the most "classical" state of light in nature for large α. As a continuous variable system, one needs to carefully consider the observables that will be used to determine whether the LGI is violated or not. Here we used the discrete Pegg–Barnett phase operator with two different binning strategies to define an observable with ± 1 values. These observables were then used to determine the two-time correlation functions necessary to test the LGI.

In the ideal situation without dissipation, we showed that the coherent state $|\alpha\rangle$ violates the LGIs over a wide parameter regime even with significant time difference τ between the measurements used to determine the two-time correlation functions. In fact, we were able to show a LGI violation in the large N limit even if we let $|\alpha|$ be large. The coherent state $|\alpha\rangle$ keeps its nonclassical properties and it cannot be described with classical theory. Further we also considered the effect of imperfect gate operations within our measurement devices and found the violation is maintained in a reduced fashion over a wide range of parameters. However, including dissipation within our model, we found as expected that the LGI violation does disappear as τ becomes large. Regimes do however still exist where a violation can be seen.

ACKNOWLEDGMENTS

This work was supported by MEXT Quantum Leap Flagship Program (MEXT Q-LEAP) Grant Number JPMXS0120351339.

Appendix A: Solutions of Eq. (1)

Let us begin by assuming that the initial state can be expressed by a density matrix made up of the component $v(0) = |\alpha\rangle\langle\beta|$, where $|\alpha\rangle$ and $|\beta\rangle$ represent the coherent states with complex amplitudes α and β. According to the master equation (1), $v(0)$ evolves as

$$v(t) = \exp\Big(-\frac{1}{2}(|\alpha|^2 + |\beta|^2 - 2\alpha\beta^*)\Big[1 - \exp[-2\Gamma t]\Big]\Big)|\alpha\exp(-i\Omega t)\rangle\langle\beta\exp(-i\Omega t)|, \tag{A1}$$

with $\Omega = \omega - i\Gamma$ [11, 29, 30]. It is useful to point out that the time evolution of the initial state $|\alpha\rangle$ is given by $|\alpha\exp(-i\Omega t)\rangle$.

Next consider that a component of the density matrix of the initial state is given by $v(0) = |n\rangle\langle m|$, where $|n\rangle$ and $|m\rangle$ represent the nth and mth Fock states. It is straightforward to show that $v(0)$ evolves as

$$v(t) = \exp[-\Gamma t(n+m) - i\omega(n-m)t] \sum_{l=0}^{\min(n,m)} \Big[\exp[2\Gamma t] - 1\Big]^l \sqrt{\binom{n}{l}\binom{m}{l}}|n-l\rangle\langle m-l|. \tag{A2}$$

Appendix B: Explicit forms of $|\psi'_{\pm}\rangle_s$ for Eqs. (23) and (24)

According to Eqs. (17) and (18), the noisy QFT transforms $|\alpha\rangle_s$ into

$$|\psi\rangle_s = C_s(\alpha)\frac{1}{2^{L/2}}\sum_{x=0}^{2^L-1}\sum_{y=0}^{2^L-1}\frac{\alpha^x}{\sqrt{x!}}\exp[i\frac{2\pi}{2^L}xy + i\sum_{p\in\{2,\ldots,L\}}\sum_{q\in\{1,\ldots L-1\},p>q,}\Delta_{pq}x_p y_{L-q+1}]|y\rangle. \tag{B1}$$

Because we want to observe $\hat{O}_s^{(+,-)}$, we should measure $|y_L\rangle$. If we detect $y_L = 0$, that is to say, $O_s^{(+,-)} = 1$, the wave function collapses from $|\psi\rangle_s$ to a non-normalized one,

$$|\psi_+\rangle_s = C_s(\alpha)\frac{1}{2^{L/2}}\sum_{x=0}^{2^L-1}\sum_{y'=0}^{2^{L-1}-1}\frac{\alpha^x}{\sqrt{x!}}\exp[i\frac{2\pi}{2^L}xy' + i\sum_{p\in\{3,\ldots,L\}}\sum_{q\in\{2,\ldots L-1\},p>q,}\Delta_{pq}x_p y'_{L-q+1}]|y'\rangle. \tag{B2}$$

In contrast, if we detect $y_L = 1$, that is to say, $O_s^{(+,-)} = -1$, the wave function collapses from $|\psi\rangle_s$ to a non-normalized one,

$$\begin{aligned}|\psi_-\rangle_s = C_s(\alpha)\frac{1}{2^{L/2}}\sum_{x=0}^{2^L-1}\sum_{y'=0}^{2^{L-1}-1}\frac{\alpha^x}{\sqrt{x!}}\exp[i\frac{2\pi}{2^L}xy' + i2\pi\frac{x}{2}\\ +i\sum_{p\in\{3,\ldots,L\}}\sum_{q\in\{2,\ldots L-1\},p>q,}\Delta_{pq}x_p y'_{L-q+1} + i\sum_{p\in\{2,\ldots,L\}}\Delta_{p1}x_p]|y'+2^{L-1}\rangle.\end{aligned} \tag{B3}$$

We can derive $||\psi_+\rangle_s|^2 = ||\psi_-\rangle_s|^2 = 1/2$ with ease.

To accomplish the QND measurement, we need to apply noisy QFT^{-1} to $|\psi_\pm\rangle_s$ and obtain $|\psi'_\pm\rangle_s$. From Eqs. (B2) and (B3), we write these explicitly as

$$\begin{aligned}|\psi'_+\rangle_s &= (\text{noisy QFT}^{-1})|\psi_+\rangle_s\\ &= \frac{C_s(\alpha)}{d}\sum_{x=0}^{d-1}\sum_{y'=0}^{(d/2)-1}\sum_{z=0}^{d-1}\frac{\alpha^x}{\sqrt{x!}}\exp\Bigg[i\frac{2\pi}{d}y'(x-z) + i\sum_{\substack{p\in\{3,\ldots,L\},\\ q\in\{2,\ldots L-1\},\\ p>q}}\Delta_{pq}x_p y'_{L-q+1}\\ &\qquad +i\sum_{\substack{p\in\{2,\ldots,L-1\},\\ q\in\{1,\ldots L-2\},\\ p>q}}\tilde{\Delta}_{pq}y'_p z_{L-q+1}\Bigg]|z\rangle,\\ |\psi'_-\rangle_s &= (\text{noisy QFT}^{-1})|\psi_-\rangle_s\\ &= \frac{C_s(\alpha)}{d}\sum_{x=0}^{d-1}\sum_{y'=0}^{(d/2)-1}\sum_{z=0}^{d-1}\frac{\alpha^x}{\sqrt{x!}}\exp\Bigg[i\frac{2\pi}{d}y'(x-z) + i\pi(x-z) + i\sum_{\substack{p\in\{3,\ldots,L\},\\ q\in\{2,\ldots L-1\},\\ p>q}}\Delta_{pq}x_p y'_{L-q+1}\\ &\qquad +i\sum_{p\in\{2,\ldots,L\}}\Delta_{p1}x_p + i\sum_{\substack{p\in\{2,\ldots,L-1\},\\ q\in\{1,\ldots L-2\},\\ p>q}}\tilde{\Delta}_{pq}y'_p z_{L-q+1}\Bigg]|z\rangle,\end{aligned} \tag{B4}$$

where $\{\Delta_{pq}\}$ and $\{\tilde{\Delta}_{pq}\}$ are Gaussian variables generated by the noisy QFT and (noisy QFT)$^{-1}$, respectively.

Appendix C: Derivation of Eqs. (26) and (27)

We prepare the coherent state $|\alpha\rangle$ as our system's initial state at $t_1 = 0$. The probability that we obtain $O_1 = +1$ at $t_1 = 0$ is given by

$$\begin{aligned}P_1(+1) &= \langle\alpha|\Pi_s^{(\text{even})}|\alpha\rangle\\ &= \sum_{m=0}^{N}|_s\langle\phi_{2m}|\alpha\rangle|^2\\ &= (s+1)^{-1}\exp(-|\alpha|^2)\sum_{m=0}^{N}\sum_{n=0}^{s}\sum_{n'=0}^{s}\exp[-i(n-n')\phi_{2m}]\tilde{\alpha}(n)\tilde{\alpha}^*(n'),\end{aligned} \tag{C1}$$

where $\tilde{\alpha}(n) = \alpha^n/\sqrt{n!}$, and $\tilde{\alpha}^*(n) = (\alpha^*)^n/\sqrt{n!}$. Here, we examine the following finite series:

$$S_1(N, n-n') = \sum_{m=0}^{N} \exp[-i(n-n')\phi_{2m}]$$
$$= \exp[-i(n-n')\phi_0] \frac{\exp[-2i(n-n')\pi] - 1}{\exp[-2i(n-n')\pi/(N+1)] - 1}. \tag{C2}$$

To evaluate the above series, we draw attention to the fact $-2N-1 \leq n-n' \leq 2N+1$. Then, we obtain

$$S_1(N, n-n') = \begin{cases} N+1 & \text{for } n = n' \\ (N+1)\exp[-i(N+1)\phi_0] & \text{for } n-n' = N+1 \\ (N+1)\exp[i(N+1)\phi_0] & \text{for } n-n' = -N-1 \\ 0 & \text{for others} \end{cases}. \tag{C3}$$

Based on the above calculations, we obtain $P_1(+1)$ as

$$P_1(+1) = \frac{1}{2}\exp(-|\alpha|^2)\{\sum_{n=0}^{s} |\tilde{\alpha}(n)|^2 + \exp[-i(N+1)\phi_0] \sum_{n=N+1}^{s} \tilde{\alpha}(n)\tilde{\alpha}^*(n-N-1)$$
$$+ \exp[i(N+1)\phi_0] \sum_{n=0}^{N} \tilde{\alpha}(n)\tilde{\alpha}^*(n+N+1)\}. \tag{C4}$$

Changing the representation of $P_1(+1)$ from Eq. (C1) to Eq. (C4), we remove the factor $(s+1)^{-1}$ because $s = 2N+1$ and $S_1(N, n-n')$ includes the factor $(N+1)$ as shown in Eq. (C3). Thus, the operation of taking large s limit does not causes any troubles.

If we observe $\Pi_s^{(\text{even})}$ at $t_1 = 0$, the wave function collapses projecting us to the non-normalized sate,

$$\Pi_s^{(\text{even})}|\alpha\rangle = \sum_{m=0}^{N} {}_s\langle\phi_{2m}|\alpha\rangle|\phi_{2m}\rangle_s$$
$$= (s+1)^{-1}\exp(-|\alpha|^2/2) \sum_{n=0}^{s}\sum_{n'=0}^{s} \tilde{\alpha}(n) \sum_{m=0}^{N} \exp[-i(n-n')\phi_{2m}]|n'\rangle$$
$$= \frac{1}{2}\exp(-|\alpha|^2/2)\{\sum_{n=0}^{s} \tilde{\alpha}(n)|n\rangle + \exp[-i(N+1)\phi_0] \sum_{n=0}^{N} \tilde{\alpha}(n+N+1)|n\rangle$$
$$+ \exp[i(N+1)\phi_0] \sum_{n=N+1}^{s} \tilde{\alpha}(n-N-1)|n\rangle\}. \tag{C5}$$

In the right-hand side of the above equation, the factor $(s+1)^{-1}$ disappears because of the same reason mentioned in Eq. (C4).

Smilarly, we obtain the probability $P_1(-1)$ if we observe $O_1 = -1$ at $t_1 = 0$ and the sate after the wave-function collapse $\Pi_s^{(\text{odd})}|\alpha\rangle$. In these derivations, the following formula is useful:

$$S_2(N, n-n') = \sum_{m=0}^{N} \exp[-i(n-n')\phi_{2m+1}]$$
$$= \exp[-i(n-n')\phi_0 - i(n-n')\frac{2\pi}{s+1}] \frac{\exp[-2i(n-n')\pi] - 1}{\exp[-2i(n-n')\pi/(N+1)] - 1}$$
$$= \begin{cases} N+1 & \text{for } n = n' \\ -(N+1)\exp[-i(N+1)\phi_0] & \text{for } n-n' = N+1 \\ -(N+1)\exp[i(N+1)\phi_0] & \text{for } n-n' = -N-1 \\ 0 & \text{for others} \end{cases}. \tag{C6}$$

From the above formula, we obtain

$$P_1(-1) = \frac{1}{2}\exp(-|\alpha|^2)\{\sum_{n=0}^{s} |\tilde{\alpha}(n)|^2 - \exp[-i(N+1)\phi_0] \sum_{n=N+1}^{s} \tilde{\alpha}(n)\tilde{\alpha}^*(n-N-1)$$
$$- \exp[i(N+1)\phi_0] \sum_{n=0}^{N} \tilde{\alpha}(n)\tilde{\alpha}^*(n+N+1)\}, \tag{C7}$$

$$\Pi_s^{(\mathrm{odd})}|\alpha\rangle = \frac{1}{2}\exp(-|\alpha|^2/2)\{\sum_{n=0}^{s}\tilde{\alpha}(n)|n\rangle - \exp[-i(N+1)\phi_0]\sum_{n=0}^{N}\tilde{\alpha}(n+N+1)|n\rangle$$
$$-\exp[i(N+1)\phi_0]\sum_{n=N+1}^{s}\tilde{\alpha}(n-N-1)|n\rangle\}. \tag{C8}$$

It is useful to describe a non-normalized state obtained by the wave-function collapse for the observation of $O_1 = \pm 1$ at $t_1 = 0$ as $w_{1\pm}(0)$. This enables us to write $w_{1\pm}(0)$ explicitly as follows:

$$\begin{aligned} w_{1\pm}(0) &= \Pi_s^{(\chi)}|\alpha\rangle\langle\alpha|\Pi_s^{(\chi)} \\ &= \frac{1}{4}\exp[-|\alpha|^2][K_1(0)+K_2(0)+K_3(0)\pm L_1(0)\pm L_2(0)+L_3(0)\pm L_1^\dagger(0)\pm L_2^\dagger(0)+L_3^\dagger(0)], \end{aligned} \tag{C9}$$

where $\chi =$ even for $w_{1+}(0)$ and odd for $w_{1-}(0)$. Further

$$\begin{aligned} K_1(0) &= \sum_{n=0}^{s}\sum_{n'=0}^{s}\tilde{\alpha}(n)\tilde{\alpha}^*(n')|n\rangle\langle n'|, \\ K_2(0) &= \sum_{n=0}^{N}\sum_{n'=0}^{N}\tilde{\alpha}(n+N+1)\tilde{\alpha}^*(n'+N+1)|n\rangle\langle n'|, \\ K_3(0) &= \sum_{n=N+1}^{s}\sum_{n'=N+1}^{s}\tilde{\alpha}(n-N-1)\tilde{\alpha}^*(n'-N-1)|n\rangle\langle n'|, \\ L_1(0) &= \exp[i(N+1)\phi_0]\sum_{n=0}^{s}\sum_{n'=0}^{N}\tilde{\alpha}(n)\tilde{\alpha}^*(n'+N+1)|n\rangle\langle n'|, \\ L_2(0) &= \exp[-i(N+1)\phi_0]\sum_{n=0}^{s}\sum_{n'=N+1}^{s}\tilde{\alpha}(n)\tilde{\alpha}^*(n'-N-1)|n\rangle\langle n'|, \\ L_3(0) &= \exp[-2i(N+1)\phi_0]\sum_{n=0}^{N}\sum_{n'=N+1}^{s}\tilde{\alpha}(n+N+1)\tilde{\alpha}^*(n'-N-1)|n\rangle\langle n'|. \end{aligned} \tag{C10}$$

We can now consider the time evolution of the state $w_{1\pm}(0)$ from $t_1 = 0$ until $t_2 = \tau$. At time τ the state has the form

$$w_{1\pm}(\tau) = \frac{1}{4}\exp[-|\alpha|^2][K_1(\tau)+K_2(\tau)+K_3(\tau)\pm L_1(\tau)\pm L_2(\tau)+L_3(\tau)\pm L_1^\dagger(\tau)\pm L_2^\dagger(\tau)+L_3^\dagger(\tau)]. \tag{C11}$$

We consider the explicit forms of $K_1(\tau)$, $K_2(\tau)$, $K_3(\tau)$, $L_1(\tau)$, $L_2(\tau)$, and $L_3(\tau)$ later.

Now we write the probability that we observe $O_1 = +1$ and $O_2 = \pm 1$ at $t_1 = 0$ and $t_2 = \tau$ as $p_{1+,2\pm}$, respectively where

$$\begin{aligned} p_{1+,2\pm} &= \mathrm{Tr}[\Pi_s^{(\chi)}w_{1+}(\tau)] \\ &= \frac{1}{4}\exp[-|\alpha|^2]\mathrm{Tr}[\Pi_s^{(\chi)}\{K_1(\tau)+K_2(\tau)+K_3(\tau) \\ &\quad +L_1(\tau)+L_2(\tau)+L_3(\tau)+L_1^\dagger(\tau)+L_2^\dagger(\tau)+L_3^\dagger(\tau)\}], \end{aligned} \tag{C12}$$

with $\chi =$ even for $p_{1+,2+}$ and odd for $p_{1+,2-}$. Similarly, we write the probability that we observe $O_1 = -1$ and $O_2 = \pm 1$ at $t_1 = 0$ and $t_2 = \tau$ as $p_{1-,2\pm}$ respectively as

$$\begin{aligned} p_{1-,2\pm} &= \mathrm{Tr}[\Pi_s^{(\chi)}w_{1-}(\tau)] \\ &= \frac{1}{4}\exp[-|\alpha|^2]\mathrm{Tr}[\Pi_s^{(\chi)}\{K_1(\tau)+K_2(\tau)+K_3(\tau) \\ &\quad -L_1(\tau)-L_2(\tau)+L_3(\tau)-L_1^\dagger(\tau)-L_2^\dagger(\tau)+L_3^\dagger(\tau)\}], \end{aligned} \tag{C13}$$

where $\chi =$ even for $p_{1-,2+}$ and odd for $p_{1-,2-}$.

Next we can write the correlation function C_{12} as

$$C_{12} = p_{1+,2+} - p_{1+,2-} - p_{1-,2+} + p_{1-,2-}, \tag{C14}$$

allowing us to obtain Eq. (26). In the computation of C_{12} according to Eq. (C14), $\mathrm{Tr}[\Pi_s^{(\chi)}(L_1(\tau)+L_2(\tau)+L_1^\dagger(\tau)+L_2^\dagger(\tau))]=2\mathrm{Re}\{\mathrm{Tr}[\Pi_s^{(\chi)}(L_1(\tau)+L_2(\tau))]\}$ and this is the reason why Eq. (26) includes only the real part of Eq. (27). Because of Eq. (26), we only need to focus on the computation of $\mathrm{Tr}[\Pi_s^{(\chi)}(L_1(\tau)+L_2(\tau))]$.

From Eqs. (A2) and (C10), we can express $L_1(\tau)$ and $L_2(\tau)$ as

$$L_1(\tau)=\exp[i(N+1)\phi_0]\sum_{n=0}^{s}\sum_{n'=0}^{N}\tilde{\alpha}(n)\tilde{\alpha}^*(n'+N+1)\exp[-\Gamma\tau(n+n')-i\omega(n-n')\tau] \times\sum_{l=0}^{\min(n,n')}\Big[\exp[2\Gamma t]-1\Big]^l\sqrt{\binom{n}{l}\binom{n'}{l}}|n-l\rangle\langle n'-l|, \quad \text{(C15)}$$

$$L_2(\tau)=\exp[-i(N+1)\phi_0]\sum_{n=0}^{s}\sum_{n'=N+1}^{s}\tilde{\alpha}(n)\tilde{\alpha}^*(n'-N-1)\exp[-\Gamma\tau(n+n')-i\omega(n-n')\tau] \times\sum_{l=0}^{\min(n,n')}\Big[\exp[2\Gamma t]-1\Big]^l\sqrt{\binom{n}{l}\binom{n'}{l}}|n-l\rangle\langle n'-l|. \quad \text{(C16)}$$

Thus, we can describe $\mathrm{Tr}[\Pi_s^{(\chi)}L_1(\tau)]$ and $\mathrm{Tr}[\Pi_s^{(\chi)}L_2(\tau)]$ for $\chi\in\{\mathrm{even},\mathrm{odd}\}$ explicitly in the form,

$$\begin{aligned}\mathrm{Tr}[\Pi_s^{(\chi)}L_1(\tau)]=&\frac{1}{2}\exp[i(N+1)\phi_0]\sum_{n=0}^{N}\tilde{\alpha}(n)\tilde{\alpha}^*(n+N+1)\\ &\pm\frac{1}{2}\sum_{n=0}^{N}|\tilde{\alpha}(n+N+1)|^2\exp[-\Gamma\tau(2n+N+1)-i\omega(N+1)\tau]\\ &\times\sum_{l=0}^{n}[\exp(2\Gamma t)-1]^l\sqrt{\binom{n+N+1}{l}\binom{n}{l}},\end{aligned} \quad \text{(C17)}$$

$$\begin{aligned}\mathrm{Tr}[\Pi_s^{(\chi)}L_2(\tau)]=&\frac{1}{2}\exp[-i(N+1)\phi_0]\sum_{n=0}^{N}\tilde{\alpha}(n+N+1)\tilde{\alpha}^*(n)\\ &\pm\frac{1}{2}\sum_{n=0}^{N}|\tilde{\alpha}(n)|^2\exp[-\Gamma\tau(2n+N+1)+i\omega(N+1)\tau]\\ &\times\sum_{l=0}^{n}[\exp(2\Gamma t)-1]^l\sqrt{\binom{n+N+1}{l}\binom{n}{l}},\end{aligned} \quad \text{(C18)}$$

where the $\pm$ symbol is replaced by the plus sign for $\chi=$ even and replaced by the minus sign for $\chi=$ odd. It is now straightforward to derive Eq. (27).

Appendix D: Derivation of Eqs. (30) and (31)

We prepare the coherent state $|\alpha\rangle$ as our system's initial state at $t_1=0$. The probability that we obtain $O_1=+1$ at $t_1=0$ is given by

$$\begin{aligned}P_1(+1)&=\langle\alpha|\Pi_s^{(+)}|\alpha\rangle\\ &=\sum_{m=0}^{N}|{}_s\langle\phi_m|\alpha\rangle|^2\\ &=(s+1)^{-1}\exp(-|\alpha|^2)\sum_{m=0}^{N}\sum_{n=0}^{s}\sum_{n'=0}^{s}\exp[-i(n-n')\phi_m]\tilde{\alpha}(n)\tilde{\alpha}^*(n').\end{aligned} \quad \text{(D1)}$$

Here, we examine the following finite series:

$$S_3(N, n-n') = \sum_{m=0}^{N} \exp[-i(n-n')\phi_m]$$
$$= \exp[-i(n-n')\phi_0] \frac{\exp[-i(n-n')\pi] - 1}{\exp[-i(n-n')\pi/(N+1)] - 1}. \tag{D2}$$

To evaluate the above series, we draw attention to the fact $-2N-1 \leq n-n' \leq 2N+1$. Then, we obtain

$$S_3(N, n-n') = \begin{cases} N+1 & \text{for } n = n' \\ 0 & \text{for } (n-n') \text{ is even and } n \neq n' \\ -2\exp[-i(n-n')\phi_0] & \\ /\{\exp[-i(n-n')\pi/(N+1)] - 1\} & \text{for } (n-n') \text{ is odd} \end{cases}. \tag{D3}$$

Based on the above calculations, we obtain $P_1(+1)$ as

$$P_1(+1) = \frac{1}{2}\exp(-|\alpha|^2) \sum_{n=0}^{s} |\tilde{\alpha}(n)|^2$$
$$+(s+1)^{-1}\exp(-|\alpha|^2) \sum_{n=0}^{s} \sum_{n'=0, n-n'=\text{odd}}^{s} (-2) \frac{\exp[-i(n-n')\phi_0]}{\exp[-i(n-n')\pi/(N+1)] - 1} \tilde{\alpha}(n)\tilde{\alpha}^*(n'). \tag{D4}$$

Changing the representation of $P_1(+1)$ from Eq. (D1) to Eq. (D4), we eliminate the factor $(s+1)^{-1}$ because $S_3(N, n-n')$ includes the factor $(N+1)$ as shown in Eq. (D3). In the second term of the right-hand side of Eq. (D4), we obtain $\exp[-i(n-n')\pi/(N+1)] - 1 \simeq -i(n-n')\pi/(N+1)$ for $N \gg 1$ and we can cancel the factor $(s+1)^{-1}$ and $(N+1)$ because of $s = 2N+1$. Thus, the operation of taking large s limit does not cause any troubles when we evaluate $P_1(+1)$. We can apply this technique to Eqs. (D5), (D7), (D8), (D10), (D15), (D16), and (31), as well.

If we observe $\Pi_s^{(+)}$ at $t_1 = 0$, our wave function collapses to the non-normalized sate,

$$\Pi_s^{(+)}|\alpha\rangle = \sum_{m=0}^{N} {}_s\langle\phi_m|\alpha\rangle|\phi_m\rangle_s$$
$$= (s+1)^{-1}\exp(-|\alpha|^2/2) \sum_{n=0}^{s} \sum_{n'=0}^{s} \tilde{\alpha}(n) \sum_{m=0}^{N} \exp[-i(n-n')\phi_m]|n'\rangle$$
$$= \frac{1}{2}\exp(-|\alpha|^2/2) \sum_{n=0}^{s} \tilde{\alpha}(n)|n\rangle$$
$$+(s+1)^{-1}\exp(-|\alpha|^2/2) \sum_{n=0}^{s} \sum_{n'=0, n-n'=\text{odd}}^{s} (-2) \frac{\exp[-i(n-n')\phi_0]}{\exp[-i(n-n')\pi/(N+1)] - 1} \tilde{\alpha}(n)|n'\rangle. \tag{D5}$$

Similarly, we obtain the probability $P_1(-1)$ if we observe $O_1 = -1$ at $t_1 = 0$ and the sate after the wave-function collapse $\Pi_s^{(-)}|\alpha\rangle$. In these derivations, the following formula is useful:

$$S_4(N, n-n') = \sum_{m=N+1}^{s} \exp[-i(n-n')\phi_m]$$
$$= \exp[-i(n-n')\phi_0 - i(n-n')\pi] \frac{\exp[-i(n-n')\pi] - 1}{\exp[-i(n-n')\pi/(N+1)] - 1}$$
$$= \begin{cases} N+1 & \text{for } n = n' \\ 0 & \text{for } (n-n') \text{ is even and } n \neq n' \\ 2\exp[-i(n-n')\phi_0] & \\ /\{\exp[-i(n-n')\pi/(N+1)] - 1\} & \text{for } (n-n') \text{ is odd} \end{cases}. \tag{D6}$$

From the above formula, we obtain

$$P_1(-1) = \frac{1}{2}\exp(-|\alpha|^2) \sum_{n=0}^{s} |\tilde{\alpha}(n)|^2$$
$$-(s+1)^{-1}\exp(-|\alpha|^2) \sum_{n=0}^{s} \sum_{n'=0, n-n'=\text{odd}}^{s} (-2) \frac{\exp[-i(n-n')\phi_0]}{\exp[-i(n-n')\pi/(N+1)] - 1} \tilde{\alpha}(n)\tilde{\alpha}^*(n'), \tag{D7}$$

$$\Pi_s^{(-)}|\alpha\rangle = \frac{1}{2}\exp(-|\alpha|^2/2)\sum_{n=0}^{s}\tilde{\alpha}(n)|n\rangle$$
$$-(s+1)^{-1}\exp(-|\alpha|^2/2)\sum_{n=0}^{s}\sum_{n'=0,n-n'=\text{odd}}^{s}(-2)\frac{\exp[-i(n-n')\phi_0]}{\exp[-i(n-n')\pi/(N+1)]-1}\tilde{\alpha}(n)|n'\rangle. \quad \text{(D8)}$$

We can now describe the non-normalized state obtained by the wave-function collapse after the observation of $O_1 = \pm 1$ at $t_1 = 0$ as

$$\begin{aligned} & w_{1\pm}(0) \\ & = \Pi_s^{(\pm)}|\alpha\rangle\langle\alpha|\Pi_s^{(\pm)} \\ & = \exp[-|\alpha|^2]\{K_1(0) \pm [L(0) + L^\dagger(0)] + K_2(0)\}, \end{aligned} \quad \text{(D9)}$$

where

$$\begin{aligned} K_1(0) &= \frac{1}{4}\sum_{n=0}^{s}\sum_{n'=0}^{s}\tilde{\alpha}(n)\tilde{\alpha}^*(n')|n\rangle\langle n'|, \\ K_2(0) &= (s+1)^{-2}\sum_{n=0}^{s}\sum_{\substack{n'=0,\\ n-n'=\text{odd}}}^{s}\sum_{m=0}^{s}\sum_{\substack{m'=0,\\ m-m'=\text{odd}}}^{s} \\ &\quad \times 4\tilde{\alpha}(n)\tilde{\alpha}^*(m)\frac{\exp[-i(n-n')\phi_0]}{\exp[-i(n-n')\pi/(N+1)]-1}\frac{\exp[i(m-m')\phi_0]}{\exp[i(m-m')\pi/(N+1)]-1}|n'\rangle\langle m'|, \\ L(0) &= \frac{1}{2}(s+1)^{-1}\sum_{n=0}^{s}\sum_{m=0}^{s}\sum_{\substack{m'=0,\\ m-m'=\text{odd}}}^{s}\tilde{\alpha}(n)\tilde{\alpha}^*(m)(-2)\frac{\exp[i(m-m')\phi_0]}{\exp[i(m-m')\pi/(N+1)]-1}|n\rangle\langle m'|. \end{aligned} \quad \text{(D10)}$$

This enables us now to consider the time evolution of the state $w_{1\pm}(0)$ from $t_1 = 0$ until $t_2 = \tau$. The resulting state has the form

$$w_{1\pm}(\tau) = \exp[-|\alpha|^2]\{K_1(\tau) \pm [L(\tau) + L^\dagger(\tau)] + K_2(\tau)\}. \quad \text{(D11)}$$

Let us now describe the probability that we observe $O_1 = +1$ and $O_2 = \pm 1$ at $t_1 = 0$ and $t_2 = \tau$ respectively as

$$\begin{aligned} p_{1+,2\pm} &= \text{Tr}[\Pi_s^{(\pm)}w_{1+}(\tau)] \\ &= \exp[-|\alpha|^2]\text{Tr}\Big[\Pi_s^{(\pm)}[K_1(\tau) + (L(\tau) + L^\dagger(\tau)) + K_2(\tau)]\Big]. \end{aligned} \quad \text{(D12)}$$

Similarly, we write the probability that we observe $O_1 = -1$ and $O_2 = \pm 1$ at $t_1 = 0$ and $t_2 = \tau$ respectively as

$$\begin{aligned} p_{1-,2\pm} &= \text{Tr}[\Pi_s^{(\pm)}w_{1-}(\tau)] \\ &= \exp[-|\alpha|^2]\text{Tr}\Big[\Pi_s^{(\pm)}[K_1(\tau) - (L(\tau) + L^\dagger(\tau)) + K_2(\tau)]\Big]. \end{aligned} \quad \text{(D13)}$$

We can now write the correlation function C_{12} as

$$C_{12} = p_{1+,2+} - p_{1+,2-} - p_{1-,2+} + p_{1-,2-}, \quad \text{(D14)}$$

and so obtain Eq. (30).

From Eqs. (A2) and (D10), we can express $L(\tau)$ as

$$\begin{aligned} L(\tau) &= \frac{1}{2}(s+1)^{-1}\sum_{n=0}^{s}\sum_{m=0}^{s}\sum_{\substack{m'=0,\\ m-m'=\text{odd}}}^{s}\tilde{\alpha}(n)\tilde{\alpha}^*(m)(-2)\frac{\exp[i(m-m')\phi_0]}{\exp[i(m-m')\pi/(N+1)]-1} \\ &\quad \times \exp[-\Gamma\tau(n+m') - i\omega(n-m')\tau]\sum_{l=0}^{\min(n,m')}\Big[\exp[2\Gamma t]-1\Big]^l\sqrt{\binom{n}{l}\binom{m'}{l}}|n-l\rangle\langle m'-l|. \end{aligned} \quad \text{(D15)}$$

Thus, we can describe $\mathrm{Tr}[\Pi_s^{(\pm)} L(\tau)]$ explicitly in the form,

$$\begin{aligned}\mathrm{Tr}[\Pi_s^{(\pm)} L(\tau)] = & \frac{1}{4}(s+1)^{-1} \sum_{m=0}^{s} \sum_{m'=0, m-m'=\mathrm{odd}}^{s} \tilde{\alpha}(m')\tilde{\alpha}^*(m)(-2)\frac{\exp[i(m-m')\phi_0]}{\exp[i(m-m')\pi/(N+1)]-1} \\ & \pm\frac{1}{2}(s+1)^{-2} \sum_{m=0}^{s} \sum_{m'=0, m-m'=\mathrm{odd}}^{s} \sum_{n=0, n-m'=\mathrm{odd}}^{s} (-2)\frac{\exp[-i(n-m')\phi_0]}{\exp[-i(n-m')\pi/(N+1)]-1} \\ & \times\tilde{\alpha}(n)\tilde{\alpha}^*(m)(-2)\frac{\exp[i(m-m')\phi_0]}{\exp[i(m-m')\pi/(N+1)]-1} \\ & \times\exp[-\Gamma\tau(n+m') - i\omega(n-m')\tau] \sum_{l=0}^{\min(n,m')} [\exp(2\Gamma t)-1]^l \sqrt{\binom{n}{l}\binom{m'}{l}}. \end{aligned} \tag{D16}$$

Based on the above calculations, we obtain Eq. (31).

[1] A. J. Leggett and A. Garg, 'Quantum mechanics versus macroscopic realism: is the flux there when nobody looks?', Phys. Rev. Lett. **54**(9), 857–860 (1985).

[2] C. Emary, N. Lambert, and F. Nori, 'Leggett–Garg inequalities', Rep. Prog. Phys. **77**(1), 016001 (2014); Rep. Prog. Phys. **77**(3), 039501 (2014).

[3] A. Einstein, B. Podolsky, and N. Rosen, 'Can quantum-mechanical description of physical reality be considered complete?', Phys. Rev. **47**(10), 777–780 (1935).

[4] O. J. E. Maroney and C. G. Timpson, 'Quantum- vs. macro- realism: what does the Leggett-Garg inequality actually test?', preprint arXiv:1412.6139 (2014).

[5] G. C. Knee, K. Kakuyanagi, M.-C. Yeh, Y. Matsuzaki, H. Toida, H. Yamaguchi, S. Saito, A. J. Leggett, and W. J. Munro, 'A strict experimental test of macroscopic realism in a superconducting flux qubit', Nat. Commun. **7**, 13253 (2016).

[6] S. V. Moreira, A. Keller, T. Coudreau, and P. Milman, 'Modeling Leggett-Garg-inequality violation', Phys. Rev. A **92**(6), 062132 (2015).

[7] L. Clemente and J. Kofler, 'No Fine theorem for macrorealism: limitations of the Leggett-Garg inequality', Phys. Rev. Lett. **116**(15), 150401 (2016).

[8] A. Fine, 'Hidden variables, joint probability, and the Bell inequalities', Phys. Rev. Lett. **48**(5), 291–295 (1982).

[9] K. Wang, G. C. Knee, X. Zhan, Z. Bian, J. Li, and P. Xue, 'Optimal experimental demonstration of error-tolerant quantum witnesses', Phys. Rev. A **95**(3), 032122 (2017).

[10] A. Friedenberger and E. Lutz, 'Assessing the quantumness of a damped two-level system', Phys. Rev. A **95**(2), 022101 (2017).

[11] H. Azuma and M. Ban, 'Violations of the Leggett–Garg inequality for coherent and cat states', Eur. Phys. J. D **75**(6), 167 (2021).

[12] A. Palacios-Laloy, F. Mallet, F. Nguyen, P. Bertet, D. Vion, D. Esteve, and A. N. Korotkov, 'Experimental violation of a Bell's inequality in time with weak measurement', Nat. Phys. **6**, 442–447 (2010).

[13] G. C. Knee, S. Simmons, E. M. Gauger, J. J. L. Morton, H. Riemann, N. V. Abrosimov, P. Becker, H.-J. Pohl, K. M. Itoh, M. L. W. Thewalt, G. A. D. Briggs, and S. C. Benjamin, 'Violation of a Leggett–Garg inequality with ideal non-invasive measurements', Nat. Commun. **3**, 606 (2012).

[14] J.-S. Xu, C.-F. Li, X.-B. Zou, and G.-C. Guo, 'Experimental violation of the Leggett–Garg inequality under decoherence', Sci. Rep. **1**, 101 (2011).

[15] G. J. Pryde, J. L. O'Brien, A. G. White, S. D. Bartlett, and T. C. Ralph, 'Measuring a photonic qubit without destroying it', Phys. Rev. Lett. **92**(19), 190402 (2004).

[16] M. E. Goggin, M. P. Almeida, M. Barbieri, B. P. Lanyon, J. L. O'Brien, A. G. White, and G. J. Pryde, 'Violation of the Leggett–Garg inequality with weak measurements of photons', Proc. Natl. Acad. Sci. USA **108**(4), 1256–1261 (2011).

[17] N. S. Williams and A. N. Jordan, 'Weak values and the Leggett-Garg inequality in solid-state qubits', Phys. Rev. Lett. **100**(2), 026804 (2008).

[18] H. Katiyar, A. Brodutch, D. Lu, and R. Laflamme, 'Experimental violation of the Leggett–Garg inequality in a three-level system', New J. Phys. **19**(2), 023033 (2017).

[19] P. A. M. Dirac, 'The quantum theory of the emission and absorption of radiation', Proc. R. Soc. Lond. A **114**(767), 243–265 (1927).

[20] L. Susskind and J. Glogower, 'Quantum mechanical phase and time operator', Phys. Phys. Fiz. **1**(1), 49–61 (1964).

[21] D. T. Pegg and S. M. Barnett, 'Unitary phase operator in quantum mechanics', Europhys. Lett. **6**(6), 483–487 (1988).

[22] D. T. Pegg and S. M. Barnett, 'Phase properties of the quantized single-mode electromagnetic field', Phys. Rev. A **39**(4), 1665–1675 (1989).

[23] S. M. Barnett and D. T. Pegg, 'On the Hermitian optical phase operator', J. Mod. Opt. **36**(1), 7–19 (1989).

[24] J. W. Noh, A. Fougères, and L. Mandel, 'Measurement of the quantum phase by photon counting', Phys. Rev. Lett. **67**(11), 1426–1429 (1991).

[25] J. W. Noh, A. Fougères, and L. Mandel, 'Operational approach to the phase of a quantum field', Phys. Rev. A **45**(1), 424–442 (1992).

[26] J. W. Noh, A. Fougères, and L. Mandel, 'Further investigations of the operationally defined quantum phase', Phys. Rev. A **46**(5), 2840–2852 (1992).

[27] M. Beck, D. T. Smithey, J. Cooper, and M. G. Raymer, 'Experimental determination of number-phase uncertainty relations', Opt. Lett. **18**(15), 1259–1261 (1993).

[28] D. T. Smithey, M. Beck, J. Cooper, and M. G. Raymer, 'Measurement of number-phase uncertainty relations of optical fields', Phys. Rev. A **48**(4), 3159–3167 (1993).

[29] D. F. Walls and G. J. Milburn, *Quantum optics* (Springer-Verlag, Berlin, 1994).

[30] S. M. Barnett and P. M. Radmore, *Methods in theoretical quantum optics* (Oxford University Press, Oxford, 1997).

[31] D. Coppersmith, 'An approximate Fourier transform useful in quantum factoring', IBM Research Report No. RC19642 (1994). [arXiv:quant-ph/0201067]

[32] A. Ekert and R. Jozsa 'Quantum computation and Shor's factoring algorithm', Rev. Mod. Phys. **68**(3), 733–753 (1996).

[33] A. Barenco, A. Ekert, K.-A. Suominen, and P. Törmä, 'Approximate quantum Fourier transform and decoherence', Phys. Rev. A **54**(1), 139–146 (1996).

[34] N. Lambert, R. Johansson, and F. Nori, 'Macrorealism inequality for optoelectromechanical systems', Phys. Rev. B **84**(24),

245421 (2011).
[35] J. Kofler and Č. Brukner, 'Classical world arising out of quantum physics under the restriction of coarse-grained measurements', Phys. Rev. Lett. **99**(18), 180403 (2007).
[36] J. Kofler and Č. Brukner, 'Conditions for quantum violation of macroscopic realism', Phys. Rev. Lett. **101**(9), 090403 (2008).
[37] C. Budroni and C. Emary, 'Temporal quantum correlations and Leggett-Garg inequalities in multilevel systems', Phys. Rev. Lett. **113**(5), 050401 (2014).
[38] V. Bužek, A. D. Wilson-Gordon, P. L. Knight, and W. K. Lai, 'Coherent states in a finite-dimensional basis: their phase properties and relationship to coherent states of light', Phys. Rev. A **45**(11), 8079–8094 (1992).